

THE LARGE APERTURE SEISMIC EXPERIMENT
PART I: DATA ACQUISITION AND ANALYSIS

by

the LASE Study Group

October 24, 1983

Preprint

TABLE OF CONTENTS

	PAGE
ABSTRACT.....	1
I. INTRODUCTION.....	2
II. DATA ACQUISITION.....	5
1. LASE CDP Profiling.....	5
2. Expanding Spread Profiles.....	9
III. DATA ANALYSIS - CDP DATA.....	12
1. Timing and Range.....	12
2. CDP Gather.....	13
3. CDP Stacks.....	16
IV. ESP DATA.....	21
1. Basic Processing.....	21
2. Derivation of Interval Velocities.....	22
3. Low Velocity Zone.....	27
CONCLUSION.....	30
REFERENCES.....	34

ABSTRACT

The developing interest in tectonic processes at passive rifted continental margins has created a need for improved knowledge of their deep geological structure, particularly in the region of the transition from oceanic to continental crust. LASE (Large Aperture Seismic Experiment) was a multi-ship, multi-institutional experiment carried out in 1981 to test and evaluate new seismic techniques for investigating the deep structure of continental margins. Using multiple shooting and receiving ships, a 13-km Common Depth Point (CDP) aperture was synthesized to improve the detection and resolution of deep reflectors. In addition, nine expanding spread profiles (ESPs), in which both reflected and refracted seismic energy are observed, were shot with airgun and explosive sources. We describe here the experimental techniques, analysis methods used and seismic results. Principal among the last is the observation of a deep 7.2 km/sec reflection event that extends across the margin and a detailed definition of the velocity structure under the prograding carbonate sequence.

I. INTRODUCTION

The LASE experiment was conducted across the Baltimore Canyon Trough, a region of the eastern U.S. margin where many other geological and geophysical investigations have been focused (Figure 1). These include stratigraphic studies using the COST B2 well drilled on the outer shelf and the COST B3 well on the slope (Scholle, 1977; 1980). These data and conventional multi-channel seismic data have heretofore provided the basis for the description of the regional stratigraphy and structure of the sedimentary basin occupying the margin (Grow et al., 1979a; Schlee, 1981). These studies suggest that the basin contains approximately 14 km of sediments beneath the outer shelf and slope, and may include sediments as old as Triassic. However, the great thickness of sediment effectively masks the basement structure, and the COST wells penetrated only to Upper Jurassic sediments. The subsidence history of the region has been described by Steckler and Watts (1978); Watts and Steckler (1979); and Sawyer et al. (1982), but these studies were limited by the lack of information on the deep structure of the margin.

Previously, the deep structure inferred from seismic refraction and gravity data (Sheridan et al., 1979; Grow et al., 1979b) provided no estimate of the depth to the crust-mantle boundary except over oceanic crust seaward of

the transition region. Gravity data have provided estimates of the deep structure in the vicinity of the ocean-continent transition, but these estimates are poorly constrained. The East Coast Magnetic Anomaly trends sub-parallel to the edge of the shelf and extends from the Blake Plateau to Nova Scotia [Klitgord and Schouten (in preparation); Klitgord and Behrendt, 1979]. It lies over the shelf in the study region, and exhibits amplitudes of 200 to 300 nT. Its position, which is thought to mark the ocean-continent transition, suggests that the transition occurs landward of the present edge of the shelf beneath the deepest part of the sedimentary basin. The cause of the magnetic anomaly is unclear, although it forms a prominent marker along the margin.

The uncertainties in the nature of the deep structure of the margin prevent a complete understanding of the processes involved in the evolution of this and other regions of the rifted margin off eastern North America. To derive new information about the deep structure of this continental margin, Lamont-Doherty Geological Observatory (L-DGO) of Columbia University, the University of Texas Marine Science Institute (UTMSI), the Woods Hole Oceanographic Institution (WHOI) and Bedford Institute of Oceanography (BIO), carried out a series of multi-channel seismic lines, using three ships to acquire large synthetic aperture profiles.

The first profiles were CDP lines (Figure 1), designed to obtain reflection information from the deepest sedimentary strata, basement and intrabasement horizons, using a 13-km synthetic aperture. This aperture was formed by arranging three ships in line and at predetermined constant offsets. By alternately firing the source arrays and recording all offset combinations, a large synthetic aperture was formed, effectively magnifying the physical array lengths (Buhl et al., 1982).

The second profiling method was designed to obtain precise velocity information for these deep strata at critical locations along the large aperture CDP lines by using two ships in the expanding spread seismic reflection/refraction method (Stoffa and Buhl, 1979).

In Part I (this paper) we describe the seismic acquisition and analysis methods used to derive information on the deep structure of the Baltimore Canyon Trough and ocean to continent transition. In Part II, we describe in detail the geological implications of these results.

II. DATA ACQUISITION

1. LASE CDP Profiling

A large synthetic aperture receiving array was deployed to focus energy from reflection interfaces at great depth within and beneath the thick sedimentary accumulations on the east coast continental margin. Conventional 2.4-3.6 km arrays do not provide sufficient normal moveout to give accurate array velocity information and often they do not receive sufficient reflection energy to produce continuous seismic images from the deeper and more complex regions of the margin. To overcome these deficiencies, three ships, the Fred Moore from UT, the Oceanus from WHOI and the Dawson from BIO were used to form a 13-km synthetic aperture.

Because of hardware availability and ship scheduling, the seismic data acquisition equipment was far from optimal. The Fred Moore was equipped with source and receiving arrays, the Dawson had only a source array, and the Oceanus was equipped with only a receiving array (Table I).

Optimizing the use of the available equipment, the ships were positioned with the Dawson in the lead, 6 km in front of the Fred Moore, while Oceanus followed the tail buoy

TABLE I

LASE ACQUISITION EQUIPMENT

DAWSON

1	Bolt 800 Airgun	2,000 in ³	
1	Bolt 1500 Airgun	<u>1,000 in³</u>	
	Total	3,000 in ³	@ 2000 PSI

MOORE

1	Bolt 800 Airgun	2,000 in ³	
1	Bolt 1500 Airgun	<u>1,000 in³</u>	
	Total	3,000 in ³	@ 2000 PSI

LRS 48 group streamer
 70 m group spacing
 30 m active / 40 m dead
 3,360 m total active length

DFS IV Data Recording System

OCEANUS

SIE 24 group streamer
 100 m group spacing
 50 m active / 50 m dead
 2,400 m total active length

WHOI Instantaneous Floating Point Data Recording System

of the Moore seismic array (Figure 2a). Seismic sources were fired alternately by the Dawson (on the minute) and the Moore (on the half-minute). Both the Moore and the Oceanus received and recorded seismic data for all the shots.

When Moore fired, it acquired conventional CDP data in the offset range of 0 to 3.6 km and Oceanus acquired data with source-receiver offsets of 3.6 to 6.0 km. When Dawson fired, Moore would record data for the source-receiver offsets of 6.0 to 9.6 km and Oceanus for the 10.0 to 13.0 km range. For safety, Oceanus remained slightly behind the Moore tailbuoy. This precaution and the space occupied by the ships and array leaders resulted in a minor loss of offset coverage.

The offset coverage of each array varied along the track because each ship moved slowly with respect to the other two. The distance between the ships at every shot was determined using Mini Ranger. Two other ranging systems, Del Norte and Raydist, failed due to space limitations or improper antenna placement. The master Mini Ranger unit was aboard the Dawson with slave units on Moore and Oceanus; consequently, there is no direct range measurement for Moore to Oceanus. These data had to be interpolated from the Dawson to Moore and Dawson to Oceanus range data.

Shot times were determined using identical National Bureau of Standards Geostationary Operational Environmental Satellite clock receivers (True Time) and back-up Systron Donner oscillators. Identical Loran-C units were also aboard all ships and used to steer the desired course. All timing, range and navigation information were logged on separate digital data logging systems for future use.

Initially it was planned to deploy a 4,000 cu.in. source array composed of a 2,000 cu.in., a 1,000 cu.in. and 2-466 cu.in. Bolt airguns. However, because of towing difficulties only the 2,000 cu.in. and 1,000 cu.in. airguns were deployed. Throughout the CDP profiling both source ships used this two-gun source array (see Table I).

After overcoming initial difficulties in keeping the ships on track and at the proper distances relative to one another, we were able to acquire four large aperture dip lines and two strike lines for a total of approximately 900 line km. LASE Line 6, which we report on here, was shot directly over USGS Line 25 (Figure 1) extending from just offshore Atlantic City to the base of the continental rise. This line received the highest acquisition and processing priority.

2. Expanding Spread Profiles

In addition to the LASE CDP lines, 9 Expanding Spread Profiles (ESPs) were successfully acquired along Line 6 (Figure 1). An expanding spread profile is a Common Mid-Point reflection/refraction survey with source-receiver offsets extending to 100 or more kilometers. In this mode of acquisition the shooting and receiving ships steam away from (or towards) a common mid-point on a fixed pre-determined course (Figure 2b). The shooting ship fires and relays the shot instant to the recording ship via radio. Seismic data are recorded aboard the receiving ship using a multi-channel array and distance is measured using Raydist, Mini Ranger, or Loran-C (for a detailed description see Stoffa and Buhl, 1979).

The ESP profiles were located to sample the continental margin at key locations: ESPs 1A ("A" for airgun), 2 and 2A were the most landward, located on what was thought to be continental crust; ESPs 3 and 3A were located on the East Coast Magnetic Anomaly; ESPs 4 and 4A were located on the Continental slope above the outer carbonate bank; and ESPs 5 and 5A were located on the upper continental rise.

At the ESP-1 location, only the airgun profile could be shot because of the shallow water depths. At each of the other four locations, however, two ESP's were shot. One

profile was acquired using the LASE airgun source array (enhanced by adding two 466 in³ airguns), and the other using 25-kg explosive charges. The ESPs were paired for several reasons. While the explosive sources produced deeply penetrating arrivals, the airguns could be fired more frequently. Also, with airgun ESPs the data could be recorded to shorter minimum offsets, producing greater resolution in the reflection data from the upper sedimentary column. In addition, these data sets enable a direct comparison of ESP results with both types of sources, providing an important baseline in the planning of future ESP work in areas where no explosive permits can be obtained.

For the explosive profiles, the shooting ship, Dawson, fired 25 kg explosive charges at 10 minute intervals. These were recorded by the receiving ship, Moore, using a digitization interval of 4 ms, and a 48-channel array with 70 m group spacing. The lines were run at a combined ship speed of 18 km/hr and resulted in contiguous offset coverage for each shot, providing essentially 100% coverage at the 70 m group spacing. The explosive ESP lines ranged from 70 to 110 km in length and were designed to provide velocity control over the entire crustal thickness, complementing the deep CDP reflection profiles.

The airgun profiles were acquired using a one-minute shooting schedule. During this time, the ships separated

only 300 m, resulting in a considerable overlap in offset coverage. In addition to providing improved resolution of the shallow structure, the profiles provided useful large offset refraction data for comparison with the explosive profiles. By combining the closely spaced shots into 50 m source-receiver offset 'bins' during processing, the signal to noise level improved significantly and deep refracted arrivals were observed for offsets up to 70 km.

III. DATA ANALYSIS - CDP DATA

1. Timing and Range

The two LASE recording ships, Moore and Oceanus, recorded the multichannel seismic data digitally on $\frac{1}{2}$ -inch, 9-track tape. The Moore recorded 48 channels in SEG-B format, using the L-DG0 DFS IV data system. The Oceanus recorded 24 channels in a modified SEG-Y format. In addition to the actual seismic data tapes, shot and record time, navigation, and the distance between ships were also recorded digitally on magnetic tape. As the first step in processing, these tapes were transcribed into a modified SEG-Y format and plots made of the raw timing and distance data. Errors in these data were found by inspection and corrected. The ranges derived from Loran-C were found to be in good agreement with the Mini Ranger ranges near shore, but they diverged farther offshore. The scatter in the Loran-derived ranges was approximately 50 m, which is reasonable since the resolution of the Loran receiver used was .1 sec or 30 m.

2. CDP Gather

Because of the unusual profiling configuration (shown in Figure 2a); i.e., two shooting ships and two recording ships, the data were handled as four separate sub-profiles. These were: 1) Moore shooting, Moore recording; 2) Moore shooting, Oceanus recording; 3) Dawson shooting, Moore recording, and 4) Dawson shooting, Oceanus recording. Each of these sub-profiles was separately CDP-gathered with its own CDP numbering scheme using the edited master data-logger tape. Ranges from the shooting to recording ships, and shot minus record time static shifts were read from the data-logger tape and input to the gathering program for each shot.

The different active group spacings of the two recording arrays (Table II) necessitated arbitrarily choosing the CDP spacing (50 m) for each of the four gathering operations. The four sub-profiles, summarized in Table III, were merged by combining the individual gathers at common geographic coordinates into "super" CDP-gathers. During this operation, the final CDP numbering system was adopted which placed CDP 1 of LASE Line 6 at 39°18' north latitude, 74°00' west longitude. Each CDP was centered at a distance of 50(CDP-1) m along a line running 126° from CDP 1. The data traces within each super gather were sorted into increasing offset order to facilitate plotting on a true offset scale. At the conclusion of the gather-merge operation, LASE Line 6 consisted of 6000 CDP gathers, each approximately 48 fold.

TABLE II

LASE ACQUISITION PARAMETERS

<u>MOORE</u>	<u>OCEANUS</u>
48 trace	24 trace
70 m groups (30 m / 40 m)	100 m groups (50 m / 50 m)
20 sec data length	20 sec data length
4 msec sampling	4 msec sampling

TABLE III

LASE CDP SORT SUMMARY

<u>MOORE-MOORE CDP SORT</u>	<u>MOORE-OCEANUS CDP SORT</u>
146 m shot spacing	146 m shot spacing
258 m offset to near group (constant)	varying offset to near group
0-3.5 km offsets	4-6.5 km offsets
50 m depth point spacing	50 m depth point spacing
16 fold	7 fold
<u>DAWSON-MOORE CDP SORT</u>	<u>DAWSON-OCEANUS CDP SORT</u>
varying shot spacing	varying shot spacing
varying offset to near group	varying offset to near group
6.5-10 km offsets	10.5-13 km offsets
50 m depth point spacing	50 m depth point spacing
16 fold	7 fold

3. CDP Stacks

Before the merged LASE gathers were further processed, variable area displays were made of the data as a function of source-receiver offset (Figure 3). Usually, three CDPs were plotted for each time-distance origin, representing the maximum data fold and a 150 m CDP bin spacing.

Figure 3 shows three CDP gathers displayed on the same time-distance graph from two areas of interest. On the left are data near the East Coast magnetic anomaly, while on the right are data from the Outer Carbonate Bank area. Many of the seismic arrivals are visibly continuous from one ship's array to the other. Each display of three CDP gathers represents the combination of 142 traces from different shot points acquired over more than one hour of data acquisition. On the shelf, wide angle reflections and refractions can be observed, as can deep reflections at approximately 6 to 9 seconds of two-way normal time.

All the data were displayed in a similar fashion and visually inspected for timing and range errors. Several incorrectly timed shot points were included in the gathers and appeared as data with a static time shift. Also, we discovered that the Dawson to Oceanus range data were incorrectly used during the initial CDP merge. (In all subsequent displays and processing steps described here these

data were excluded, since to recover the correct offsets, the data must be re-gathered.)

After editing, standard hyperbolic X-T semblance velocity scans were made to define the stacking velocities. Semblance was computed for the offset ranges 0-4 km and 0-10 km. Three CDPs were used in each velocity scan and the calculation was done every 20 CDPs. Velocities of 1400 to 6000 m/sec were scanned at an interval of 50 m/sec (Figure 4).

Both the 0-4 km and 0-10 km hyperbolic velocity scans were used to determine stacking velocities. The 0-10 km scans were unusable for the shallow part of the section (less than four seconds of two-way normal time) because of the failure of the hyperbolic travelttime assumption and the presence of refractions. Consequently, the 0-4 km scans were used for the shallow part of the section (0-4 seconds of reflection time) and the 0-10 km scans were used for the deeper part (4-16 seconds of reflection time). In all cases, Grow's (USGS unpublished) velocities for USGS Line 25 were used as a guide in the interpretation.

After stacking velocities were defined, the CDP gathers were corrected for normal moveout and displayed. This was done approximately every 100 CDPs for quality control and to define post normal moveout mutes. The mutes were defined in

table form and were spatially interpolated between analysis points along the line when the data were stacked. In most cases, offsets greater than 4 m were included in the CDP stack below approximately 4.5 seconds of two-way normal time.

Before stack, gain proportional to arrival time ($T^{1.5}$) and trace equalization (based on the mean absolute value) were applied to the data. To collapse the source waveform, predictive deconvolution was performed using a 200 msec filter with a 30 msec prediction distance and 1% white noise. A design gate of 5500 msec, beginning at 2500 msec traveltime and varying linearly with offset, was used to avoid water-borne energy.

The CDP data for source-receiver offsets of 0-10 km were stacked individually with the stacking velocities spatially interpolated between the analysis points. After stack, many post-processing sequences were tried. The sequence used in Figure 5 included a zero phase time varying band pass filter whose cut-off frequencies were:

12	and	50	Hz	at	0	msecs
10	and	40	Hz	at	3000	msecs
6	and	25	Hz	at	5000	msecs
4	and	15	Hz	at	9000	msecs
4	and	10	Hz	at	14000	msecs

In this display, which has the velocity functions derived from the ESPs superimposed, a running mix of nine traces was used to improve the definition of the deep structure, followed by spatial decimation by a factor of 3. Thus, a CDP spacing of 150 m was used for display but each trace has been averaged over 450 m. Post-stack predictive deconvolution was also applied to reduce both source and water column reverberation.

In Figure 5, it is possible to trace the top of the deep 7.2 km/sec layer from ESP 1, where it is found to lie at a two-way normal time of approximately 7.4 seconds to ESPs 2 and 3 where it is present at times greater than approximately 8.0 seconds (see Part II for a detailed interpretation). On the right part of the section, oceanic basement can be visually traced landward to approximately CDP 3300. Figure 6 is a schematic interpretation of this section showing the major geologic horizons observed in the record section, and the magnetics.

The identical processing sequence (pre and post stack) and display were used for the conventional CDP data acquired by the Moore for the offsets of 0-4 km. Figure 7 is a detailed comparison of the two record sections from the outer carbonate bank area. In this figure the additional signal to noise improvement provided by using the larger offset data (lower panel) is evident in at least two ways. First, the

residual multiple energy has been reduced to the extent that part of the prograding carbonate sequence can be traced between CDPs 2100 to 2450 at two-way times of 4.0 to 4.5 seconds. An even shallower reflection at 3.8 seconds of traveltime under the reef complex can be traced landward through the multiple to CDP 2100. It is also clear that the top of the prograding carbonate sequence is better delineated in the 0-10 km stacked section. Because of the post-normal movement mutes applied, the full 10 km aperture is not being used at these two-way times, but sufficient additional primary reflection energy is being included in the stack to give significantly better multiple attenuation and signal to random noise improvement. A similar improvement is observed on the shelf where the additional attenuation of intrabed multiples makes it possible to identify the 7.2 km/sec reflector in Figures 5 and 6.

The LASE Line 6 data were migrated (after stack) using the phase-shift method (Gazdag, 1978; Dubrulle and Gazdag, 1979). The phase shift method is a modification of the more common f-k migration (Stolt, 1978), which eliminates the extreme stretch necessary to put the data into a constant velocity versus depth form. We migrated LASE Line 6 from CDP 1000 to CDP 3000, a traverse of 100 km, using data from 0 to 16 sec. The velocity structure used was a combination of converted stacking velocities in the upper part of the

section, tied to velocity results from the expanding spread profiles for the deeper layers. Figure 8 is a comparison of the migrated and unmigrated data from the basement fault area. In the migrated record section (right), the long diffraction events present in the stacked section (left) have been substantially reduced. It is now quite clear that at 6.5 seconds of two-way time, CDP 1250 marks the edge of what we interpret as a basement normal fault (see Part II for discussion). Shallower faulting at 5.8 seconds of two-way time is also well defined in the migrated section. On the lower right of both sections the downward thrown block is clearly observed.

IV. ESP DATA

1. Basic Processing

For all nine ESPs, time and source-receiver offsets were displayed and corrected. The airgun profiles needed few or no timing corrections. In contrast, the explosive profiles required significant shot instant time corrections. Source-receiver offsets for the near offset ranges (0-40 km) were determined using Mini Ranger. As the offset increased, latitude and longitude measurements from Loran-C were incorporated into the distance determination (Loran time delays and Mini Ranger were calibrated for the near offsets, and then Loran used after the Mini Ranger's range was exceeded).

The separation rate of the ships during the airgun ESPs was approximately 18 km/hr or 300 m/minute. A one-minute firing schedule and a 3.36 km receiving array resulted in approximately 90% overlap in the source-receiver offsets between shots. Rather than maintain the original data fold, the data traces were summed into 50 m offset bins and scaled by the number of traces in each bin. Instead of a simple mix, each data trace was linearly "moved out" with a reducing velocity of 8 km/sec before summing to correct for the difference in distance between the nearest 50-m bin mid-point

and the data traces' true offset. This procedure reduced the volume of data and increased the signal to random noise level by a factor of 3.

2. Derivation of Interval Velocities

Interval velocities were derived from the LASE ESP data by analyzing seismic travel time trajectories in both the $T(X)$ and τ - p domain. Both near-vertical incidence reflections (for the airgun profiles) and wide angle reflections and refractions were used. The airgun profiles were initially analyzed in the τ - p domain and the velocity structure was refined by raytracing and comparison with the observed $T(x)$ data. Using the airgun results for the shallower part of the section, the explosive ESP data were then fitted by an iterative process of comparison with ray-traced arrivals in order to obtain interval velocities for the deep section. The seismogram density afforded by the multichannel array allowed the use of many phases in addition to the usual first arrivals.

We chose ESP 3A (Figure 9a) to illustrate in detail the method of analysis for the airgun Expanding Spread Profiles. The $T(X)$ data for source-receiver offsets of 0-20 km were transformed to the τ - p domain using data with a ray parameter sampling interval of 2 msec/km. The

locations of critically refracted and postcritically reflected arrivals were digitized and inverted to obtain $V(Z)$ by the slope-intercept or "Tau-Sum" method (Diebold & Stoffa, 1981). By picking closely-spaced tau-p points, an accurate representation of velocities and gradients in the upper seven kilometers of the section was obtained. The tau-p interval velocity model we derived was smoothed and then verified by comparing ray traced $T(X)$ arrival times with the original data.

Next, T^2-X^2 solutions were calculated for reflections with two-way normal times of 2 to 6 seconds. The very wide angles of reflection that were obtained precluded the effective use of Dix's approximation for velocity determinations. The "straight line" assumed in Dix's approximation to T^2-X^2 data is actually a curve with gentle negative curvature, becoming more curved as the velocity contrast increases. If straight lines are fitted at near-vertical incidence, most of the data are unused, resulting in a loss of velocity resolution. The curvature in the T^2-X^2 data can be eliminated if each layer is isolated and treated as a single constant-velocity layer. This is accomplished by solving for each layer step-wise from the top down and using the solutions from the overlying layers to "strip" off all the time to a given reflector that is not in the immediately superjacent layer, as described by Le Pichon et al. (1968).

Before the T^2-X^2 analysis of ESP 3A was performed, the data were phase velocity filtered to minimize the interference of the seafloor reflection and multiples, then deconvolved and displayed (Figure 9b). Compared to the original data, the wide angle reflections are readily observed; these events were used in the T^2-X^2 velocity analysis.

Finally, the derived velocity functions were reconciled and rechecked by raytracing and comparison with the original airgun and explosive ESP data. As shown in the composite velocity profile (Figure 10), the tau-p results from 0-4 seconds show more resolution in velocity than the T^2-X^2 solution, though the two results match well overall. The tau-p solution, however, produced no information as deep as the low velocity zone between 5 and 6.5 seconds. In this region, the T^2-X^2 and explosive $T(X)$ results (described below) match quite well. Below 6.5 seconds, all the information comes from the explosive ESP results described below.

Airgun ESP 4A (Figure 11a) was analyzed in a similar way. First, the data were transformed to the tau-p domain, using offsets of 0 to 20 km, then deconvolved and inverted using the Tau-Sum method. For this profile the velocity depth structure was refined by moving out the tau-p data (Figure 11b), until the reflection trajectories became

horizontal (Stoffa et al., 1981). T(X) raytracing was also performed and the event times reconciled with the data for both the airgun and explosive profiles.

ESPs 1A, 2A and 5A were analyzed in a similar fashion. The derived velocity-depth functions, after being combined with the explosive profile results, are summarized in Figure 5 and discussed in detail in Part II of the paper.

ESPs 2, 3, 4 and 5, which were shot with 25 kg explosive sources, were analyzed to produce the deep parts of the velocity functions shown in Figure 5. To illustrate this process we describe the analysis of ESP 2 (Figure 12).

In general, the minimum source-receiver offset and source characteristics of the explosive ESPs are such that the data are of little use for detailed resolution of the upper sedimentary column. The source levels, however, are great enough that arrivals from deeper horizons can be seen at large offsets, complementing the airgun ESP data.

Velocity functions for the explosive ESPs were derived by forward traveltimes modeling. Starting with the velocity models for the upper sedimentary column, which were obtained from the airgun data as described above, the deep velocity functions were developed, layer by layer, from the top down. This was an iterative process of trial and error, in which traveltimes for a given model were predicted by

analytic raytracing, displayed graphically, and compared to the data. The model was then altered until a satisfactory fit was obtained. The raytracing was performed assuming laterally homogeneous layers having velocity gradients which were linear with depth. Vertically homogeneous layers and velocity discontinuities could be included to increase modeling flexibility. Since critical points were indicated in the raytraced traveltimes solutions, some amplitude information was included in the interpretation in a subjective way.

ESP 2 is the most landward of the explosive ESPs (Figure 1). As shown in Figure 12, the minimum offset in the T-X data is 6 km, and continuous first arrivals are not seen until 12 km, due to mismatches in shot and receiver timing. The top 2.5 seconds of the velocity model are, therefore, constrained only by the ESP 2A airgun data. Between 12 and 67 km, the explosive ESP 2 data contain a large number of arrivals with greatly variable phase velocities and amplitudes.

The velocity function between 2.5 and 4.5 seconds of two-way time was determined by matching first arrivals. The points at which the modeled arrivals must cross were defined by breaks in slope of the data first arrivals, and the velocity gradients were controlled by arrival curvatures, as well as the range of offsets over which they are seen with

appreciable amplitude. Beyond 30 km; secondary arrivals played an important part in determining the velocity function. In some cases, such as the reflection from the 7.2 km/sec layer just below 8 seconds of two-way time, coherent arrivals can be followed over a range of 30 km or more. In addition, the airgun ESP 2A data were fan filtered, as described above for ESP 3A. This process revealed near vertical reflections between 4 and 8.2 seconds which could be correlated with wide angle arrivals in ESP 2. The resulting leverage strongly constrains the velocity function.

3. Low Velocity Zone

The velocity functions derived from ESP's 2, 3 and 4 contain a low velocity zone below the prograding carbonate sequence (Figure 6). Reflected arrivals from above and below this zone are particularly well developed in ESP 3A between 5 and 6.5 seconds of two-way normal time. To establish the existence of this zone, the ESP 3A data were corrected for normal moveout and displayed. To obtain the NMO velocities, the final interval velocity-depth function was converted to stacking velocities and two-way normal times. This conversion was accomplished by raytracing the velocity model (Figure 10), and finding the best-fitting hyperbolae over the area of interest by least squares. In this case, 20 km were

used in the least squares fit. The NMO corrected reflection data for the event at 6.5 seconds of traveltime now follow a nearly horizontal $X-T_0$ trajectory indicating that the stacking velocities are correct (Figure 13 left).

To test sensitivity to the low interval velocity zone, the stacking velocities were re-computed. Instead of the low velocity, an interval velocity of 6 km/sec, (equivalent to that just above the low velocity zone) was used. The data were again corrected for normal moveout and compared. The data on the left (low velocity zone) follow a nearly horizontal trajectory while the data on the right (continued high velocity) are clearly undercorrected. This is exactly the error that we would expect from using the higher stacking velocity associated with the incorrect high interval velocity for this zone.

It is apparent in Figure 13 that the stacking velocity obtained for the low velocity zone is still a bit too high. The reason for this is seen in Figure 10, where the T^2-X^2 and explosive ESP derived velocity functions are superimposed. The T^2-X^2 inversion, obtained from the reflector itself, and thus confined to offsets from 0-20 km yields a velocity function which is lower, on the average, than that produced by the explosive ESP inversion where the derived velocity function is controlled by refractions seen from offsets of 50-90 km. The resulting difference in the raytraced derived

stacking velocities (4525 m/sec vs. 4610 m/sec) causes the residual NMO in Figure 13 (left). This implies that the velocity structure within the low velocity zone is more stratified than the simple functions shown in Figure 10, and that the velocity differences are thus angle- and, therefore, offset-dependent.

Existence of the Low Velocity Zone is also supported by the interpretation of the Explosive ESP data. In ESP 2 the return from the top of the zone is seen as a first arrival beyond 37 km (Figure 12). This arrival dies out rapidly, indicating the presence of a velocity gradient. The transition at the top of the LVZ is probably not a sharp one, since no reflection was seen in the fan filtered 2A data. The bottom of the zone is seen in the fan filtered data, and can be seen in the explosive data after 14 km, as a reflection with a two-way time of approximately 6.5 seconds. This reflection, as well as phases from deeper layers, is never seen as a first arrival, but is easily defined due to the data density.

CONCLUSION

The LASE experiment succeeded in proving the feasibility of acquiring large synthetic-aperture CDP data even when the acquisition equipment available is far from optimum. The stacked 0-10 km CDP data shows an improved signal to noise ratio compared to the stacked 0-4 km Moore-to-Moore data over the deep part of the section. This improvement is due primarily to better attenuation of water column and interbed multiples.

Of particular importance is that the 7.2 km/sec layer, determined from the ESP data, can now be detected for the first time in the stacked record section. Although this event is not readily observed on USGS Line 25, it is primarily because of the correlation with the new ESP data that we are confident in our interpretation of this event in the 0-10 km stacked section.

The ESP data, both airgun and explosive, have proved invaluable in deriving the geologic interpretation described in Part II of this paper. The airgun profiles, which were particularly well suited for the shallower part of the section, also proved useful for deriving information about the deep part of the section. The additional signal level provided by the nine-fold combination of traces in these densely shot profiles indicates that even in seismically

difficult areas significant penetration is possible using airguns. Employment of a higher energy source array should make this approach viable in areas where explosives would normally be employed.

The LASE explosive ESP profiles provided most of the information for the deep part of the section, particularly the observation of the 7.2 km/sec reflection event. Because of the sparser shot spacing, these profiles poorly resolved the shallow part of the section, but the higher energy source did provide sufficient signal level so that wide angle reflection and refraction events could be observed at source-receiver offsets of up to 100 km.

The combination of the large aperture CDP data, with both the airgun and explosive ESPs, has provided a data set, which for deep crustal studies, is significantly more detailed than previously available. It is this combination which leads to the interpretation outlined in Part II of this paper.

**The institutions and principal contributors to
the LASE Study Group are:**

C. Keen, I. Reid, J. Woodside, B. Nichols
Atlantic Geoscience Centre, Bedford Institute of
Oceanography
Dartmouth, Nova Scotia, Canada

J. Ewing, P. Stoffa, D. McCowan, J. Diebold,
M. Truchan, T. O'Brien
Center for Marine Crustal Studies, Gulf Research &
Development Co.
One Blue Hill Plaza, Pearl River, New York

P. Buhl, J. Mutter, R. Mithal, J. Alsop
Lamont-Doherty Geological Observatory of Columbia
University
Palisades, New York

J. D. Phillips, T. Stark
University of Texas, Institute for Geophysics
Austin, Texas

M. Purdy, Hans Shouten
Woods Hole Oceanographic Institution
Woods Hole, Massachusetts

This work was supported by grant from the National Science Foundation, OCE 79-22884, and the industrial participants of the Ocean Margin Drilling Program:

Atlantic Richfield
Cheveron
City Service Co.
Conoco
Exxon
Mobil
Penzoil
Phillips Petroleum
Sunmark
Union Oil

and
Gulf Research & Development Company.

Canadian participation in this study was funded by Energy, Mines and Resources, through an OERD Grant to the Geological Survey of Canada.

REFERENCES

- Buhl, P., J. B. Diebold and P. L. Stoffa, "Array Length Magnification through the Use of Multiple Sources and Receiving Arrays;" Geophysics, Vol. 47, No. 3, March, 1982, pp. 311-315.
- Diebold, J. B. and P. L. Stoffa, "The Traveltime Equation, Tau-p Mapping and Inversion of Common Midpoint Data;" Geophysics, Vol. 46, No. 3, 1981, pp. 238-254.
- Dubrulle, A. A., and J. Gazdag, Migration by phase shift - An algorithmic description for array processors, Geophysics, v. 44, 1979, 1661-1666.
- Gazdag, J., Wave equation migration with the phase shift method, Geophysics, v. 43, 1978, 1342-1351.
- Grow, J. A., C. O., Bowin, D. R. Hutchinson, "The gravity field of the U.S. Atlantic continental margin," Tectonophysics, 59, 1979a, pp. 27-52.
- Grow, J. A., R. E. Mattick, J. S. Schlee, "Multichannel seismic depth sections and interval velocities over outer continental shelf and upper continental slope between Cape Hatteras and Cape Cod, in Geological and geophysical investigations of continental margins," edited by P. W. W. Dickerson, U. S. Geol. Surv. Circular, 833, 1979b, pp. 117-125.
- Klitgord, K. D. and J. C. Behrendt, in "Geological and Geophysical Investigations of Continental Margins," J. S. Watkins, L. Montadert and P. Dickerson, editors, Amer. Assoc. Petrol. Geol. Memoir, 29, 1979, p. 85.
- Le Pichon, X., R. Houtz, and J. Ewing, "Deep-sea sediment velocity determination made while reflection profiling," J. Geophys. Res., 1968, pp. 2597-2614.
- Sawyer, D. S., B. A. Swift, J. G. Sclater, and M. N. Toksoz, Geology, 10, 1982, p. 134.
- Schlee, J. S., Amer. Assoc. Petrol. Geol. Bull., 65, 1981, p. 26.
- Scholle, P. A., (ed.), "Geological Studies on the COST B-2 Well," U. S. Geol. Survey Circular, 750, 1977, 71p.

- Scholle, P. A. (ed.), "Geological Studies of the COST No. B-3 Well," U. S. Geol. Survey Circular, 883, 1980, 132p.
- Sheridan, R. E., J. A. Grow, J. C. Behrendt, and K. C. Bayer, Tectonophysics, 59, 1979, p. 1.
- Steckler, M. S. and A. B. Watts, Subsidence of the Atlantic-type continental margin off New York," Earth Planet, Science Letters, 41, 1978, pp. 1-13.
- Stoffa, P. L. and P. Buhl, "Two-Ship Multichannel Seismic Experiments for Deep Crustal Studies: Expanded Spread and Constant Offset Profiles," Journal of Geophysical Research, v. 84, 1979, pp. 7645-7660. L-DG0 Contribution No. 2860.
- Stoffa, P. L., J. B. Diebold and P. Buhl, "Inversion of Seismic Data in the Tau-p Plane," Geophys. Res., Ltrs., v. 8, no. 8, 1981, pp. 869-872.
- Stolt, R. H., "Migration by Fourier transform," Geophysics, v. 43, 1978, pp. 23-48.
- Watts, A. B. and M. S. Steckler, in "Deep Drilling Results in the Atlantic Ocean: Continental Margin and Paleoenvironments," M. Talwani, W. Hay and W. B. F. Ryan, editors, Maurice Ewing Series 3, 1979, Amer. Geophys. Union, Washington, DC, p. 218.

Figure 1 Track chart - showing the location of LASE Line 6 and the nine expanding spread profiles. The shaded area defines the location of the East Coast Magnetic Anomaly.

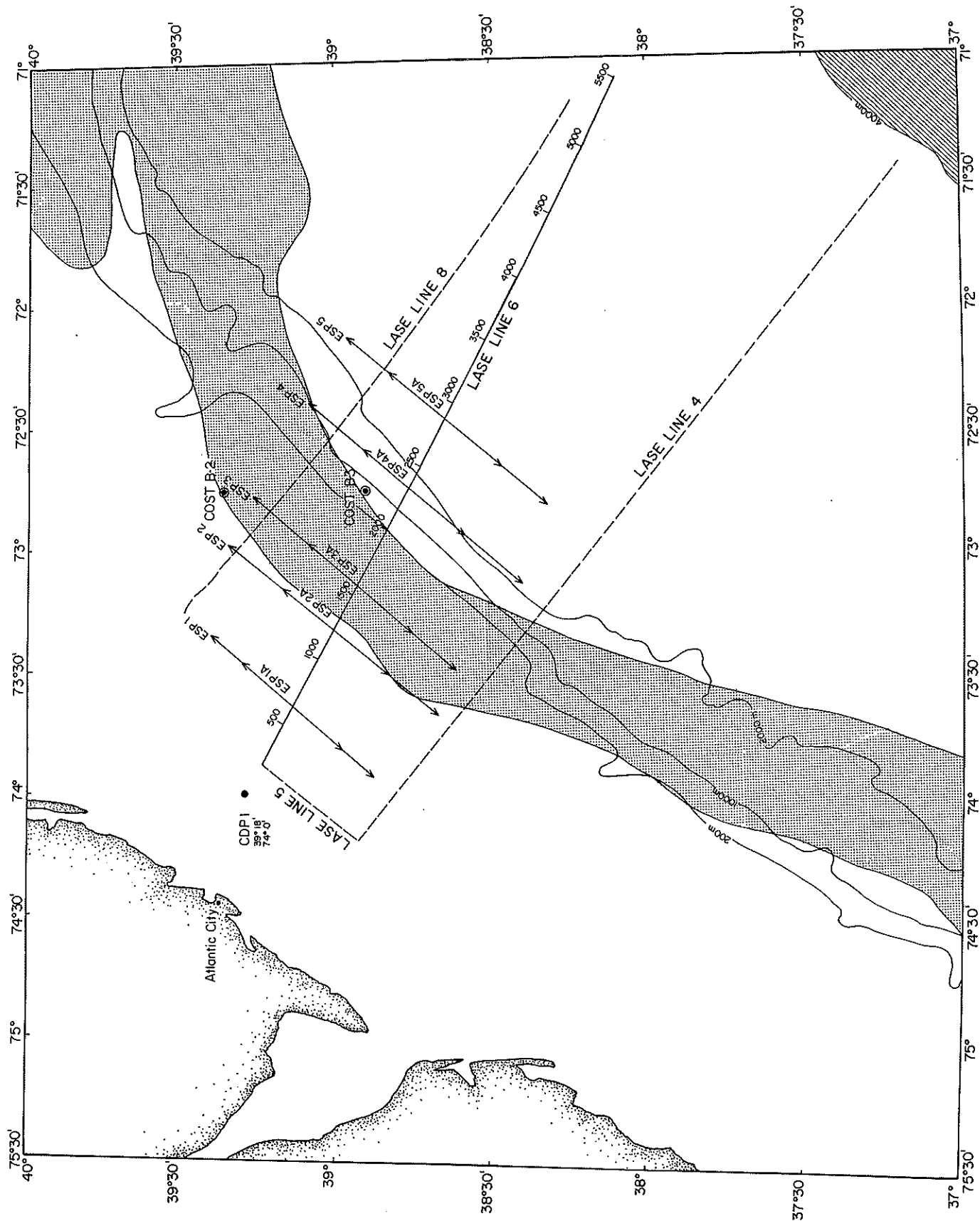


FIGURE 1

Figure 2a Schematic diagram of the LASE large aperture CDP profiling plan. The lead-ship Dawson was approximately 6.5 km ahead of Fred Moore and Oceanus followed the tailbuoy of the Moore. Range between the ships was determined using Mini-Ranger. When the Fred Moore would fire its airguns, the Moore and Oceanus would record seismic data. Moore would acquire a conventional reflection record section with offsets of 0 to 3.5 km. At the same time Oceanus would record data with offsets of approximately 3.6 to 6.0 km. Thirty seconds after the shot from Moore, Dawson would fire its airguns. Then the Fred Moore would record data with offsets from 6 to 9.6 km and the Oceanus would record offsets from 10 to 13.0 km. After initial logistical problems the ships were able to maintain the desired separation and steamed the same line using identical Loran-C receivers for navigation.

LASE EXPERIMENT CONFIGURATION

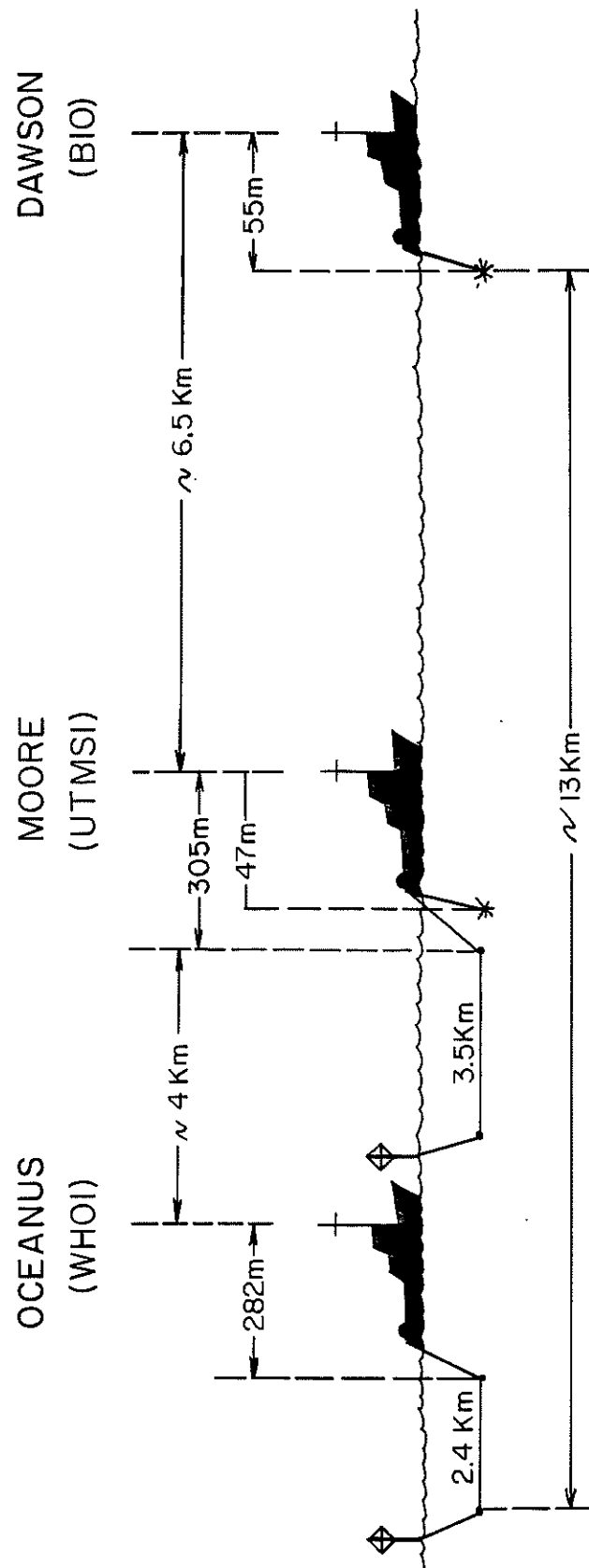


FIGURE 2a

Figure 2b Schematic diagram of how an expanding spread profile is acquired: Two ships, equipped with source arrays, depart from the common midpoint on a predetermined course. During LASE only one ship was quipped with an array, Fred Moore, while the Dawson fired either explosives or airguns. Distance between the ships was determined using Mini-Ranger and Loran-C.

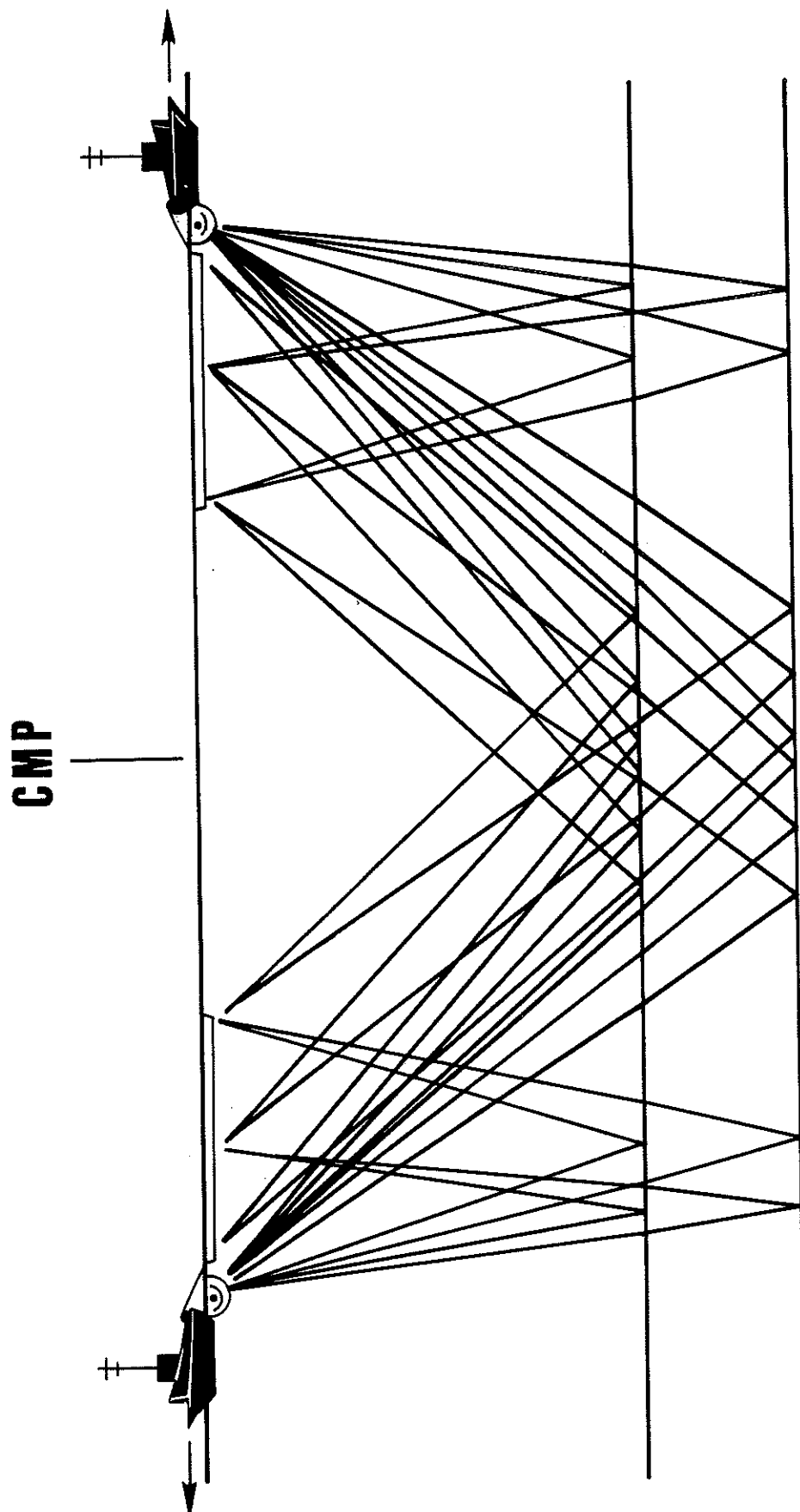


FIGURE 2b

Figure 3 LASE 0-10 km CDP gathers plotted at their true source-receiver offset from the area of the East Coast Magnetic Anomaly (left) and carbonate bank area (right). Three CDPs are displayed on each panel corresponding to a CDP ground spacing of 150 m.

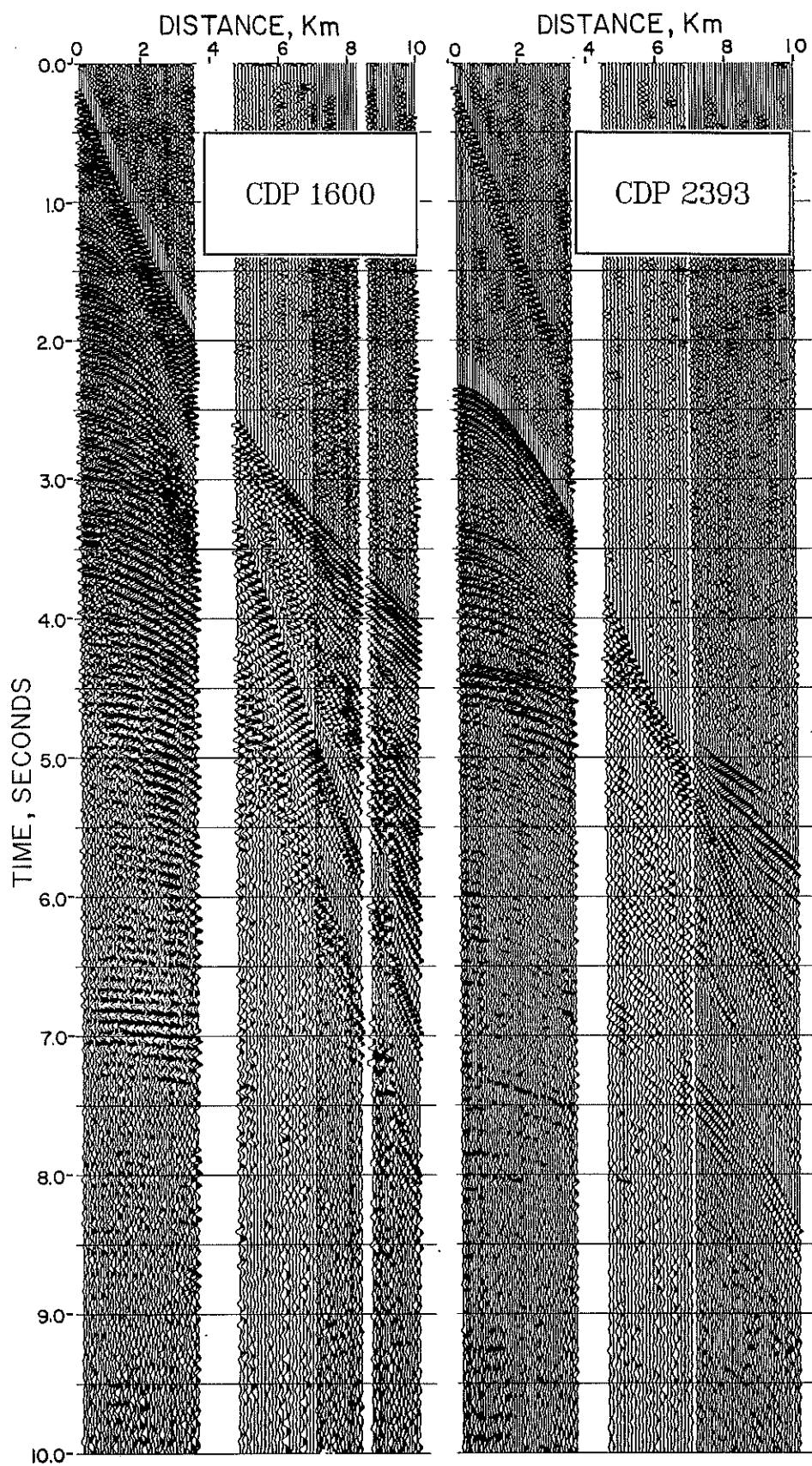


FIGURE 3

Figure 4 0-4 km (left) and 0-10 km (right) hyperbolic semblance velocity scans for LASE CDP gathers near the shelf edge. The array velocity for the reflection from the top of the carbonate sequence at 4.2 seconds of traveltime is better resolved in the 0-10 km scan, but the array velocities from the shallow part of the section are best defined from the 0-4 km velocity scan.

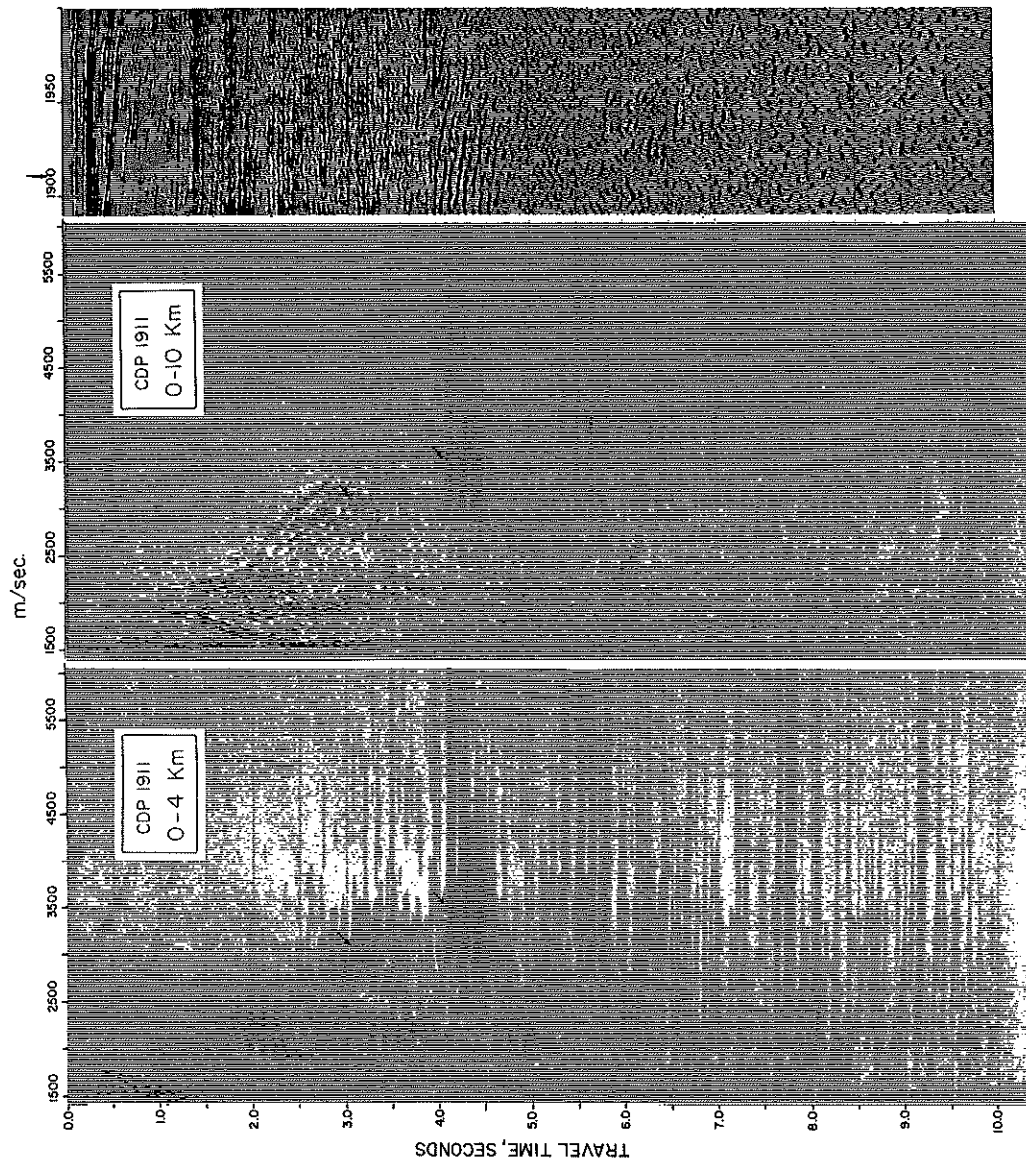


FIGURE 4

Figure 5 LASE Line 6 stacked record section with the velocity functions derived from the ESPs superimposed. Below approximately 4.5 seconds of two-way normal time source-receiver offsets of 0-10 km are included in the stack. A 750 msec AGC and time-varying bandpass filter were applied to enhance the deep reflection events. The stacked data were also mixed by a factor of 9 and spatially decimated by a factor of 3 to further increase the signal to noise level at depth.

LASE line 6

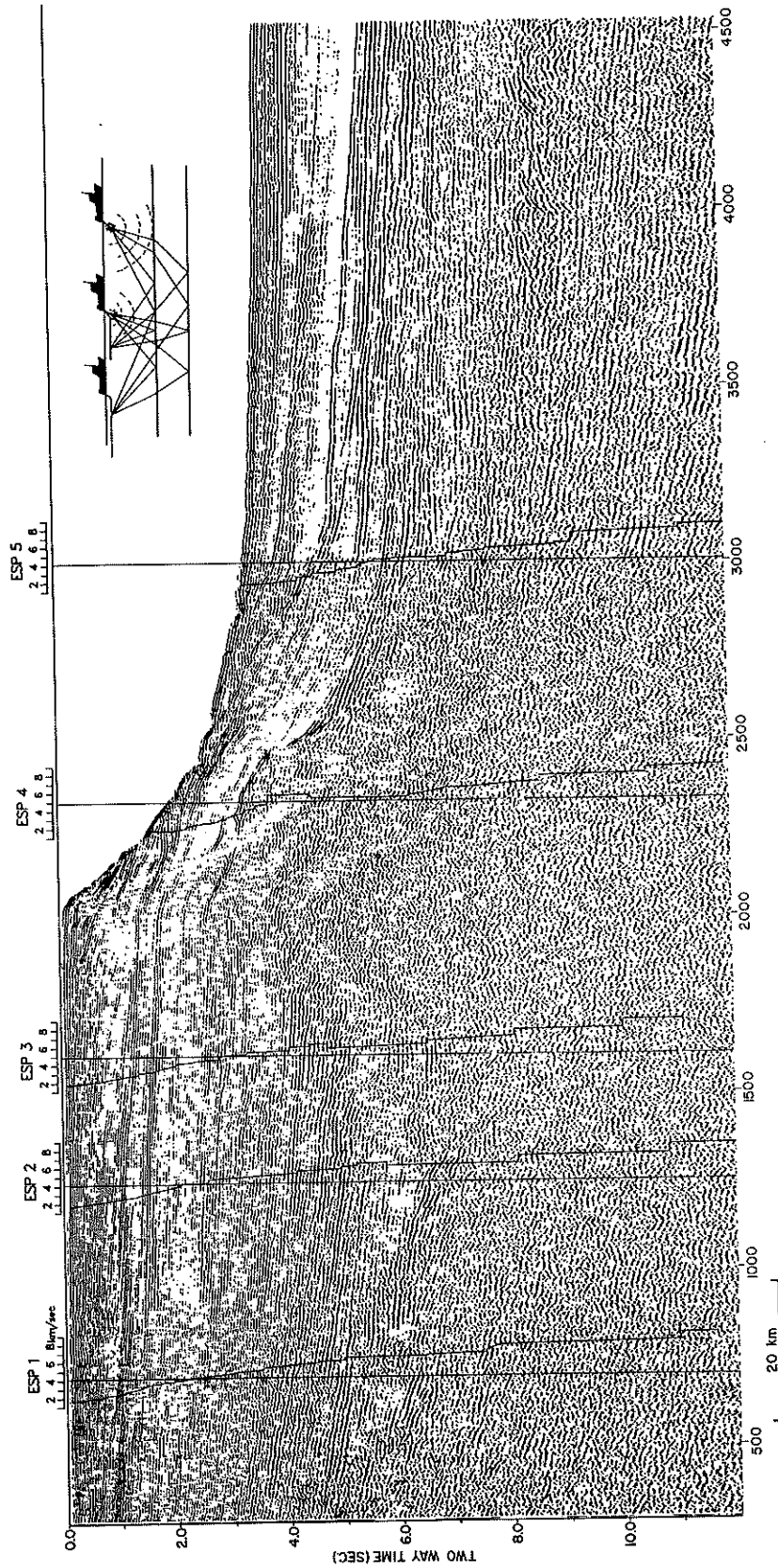


FIGURE 5

Figure 6

Schematic interpretation of the stacked record section of Figure 5. The dashed lines indicate the area between the ESPs where identification of oceanic basement and the 7.2 km/sec reflection event became difficult.

LASE line 6

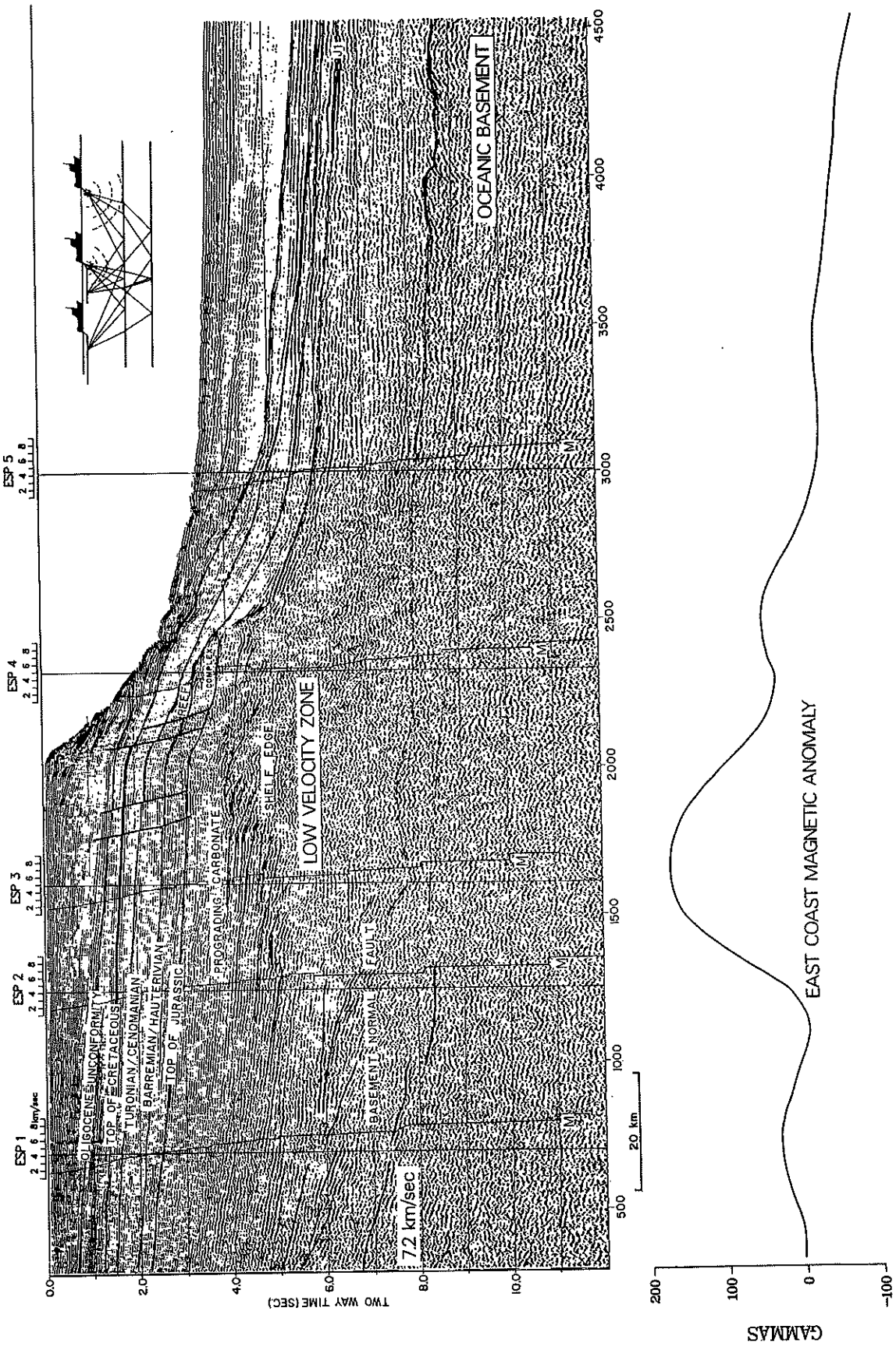


FIGURE 6

Figure 7 Comparison of the 0-4 km CDP stacked record section (upper) and 0-10 km CDP stacked record section (lower) from the Outer Carbonate Bank area. The improved multiple attenuation in the 0-10 km stack makes it possible to trace the reflectors under the reef complex landward.

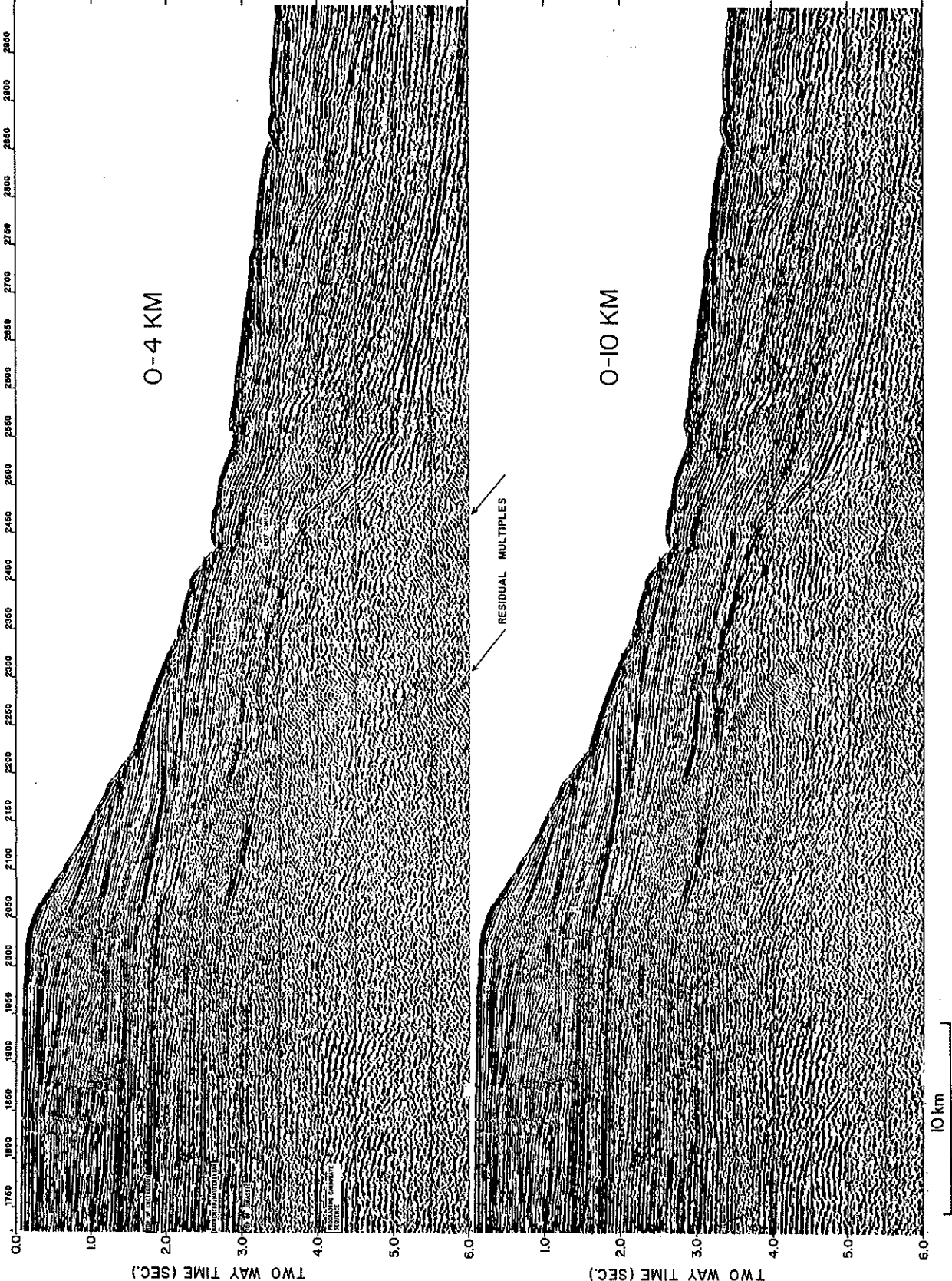


FIGURE 7

Figure 8 0-10 km stacked CDP record section (left) and after migration (right). After migration it is clear that CDP 1250 marks the edge of a basement normal fault at 6.5 seconds of traveltime.

LASE
LINE 6

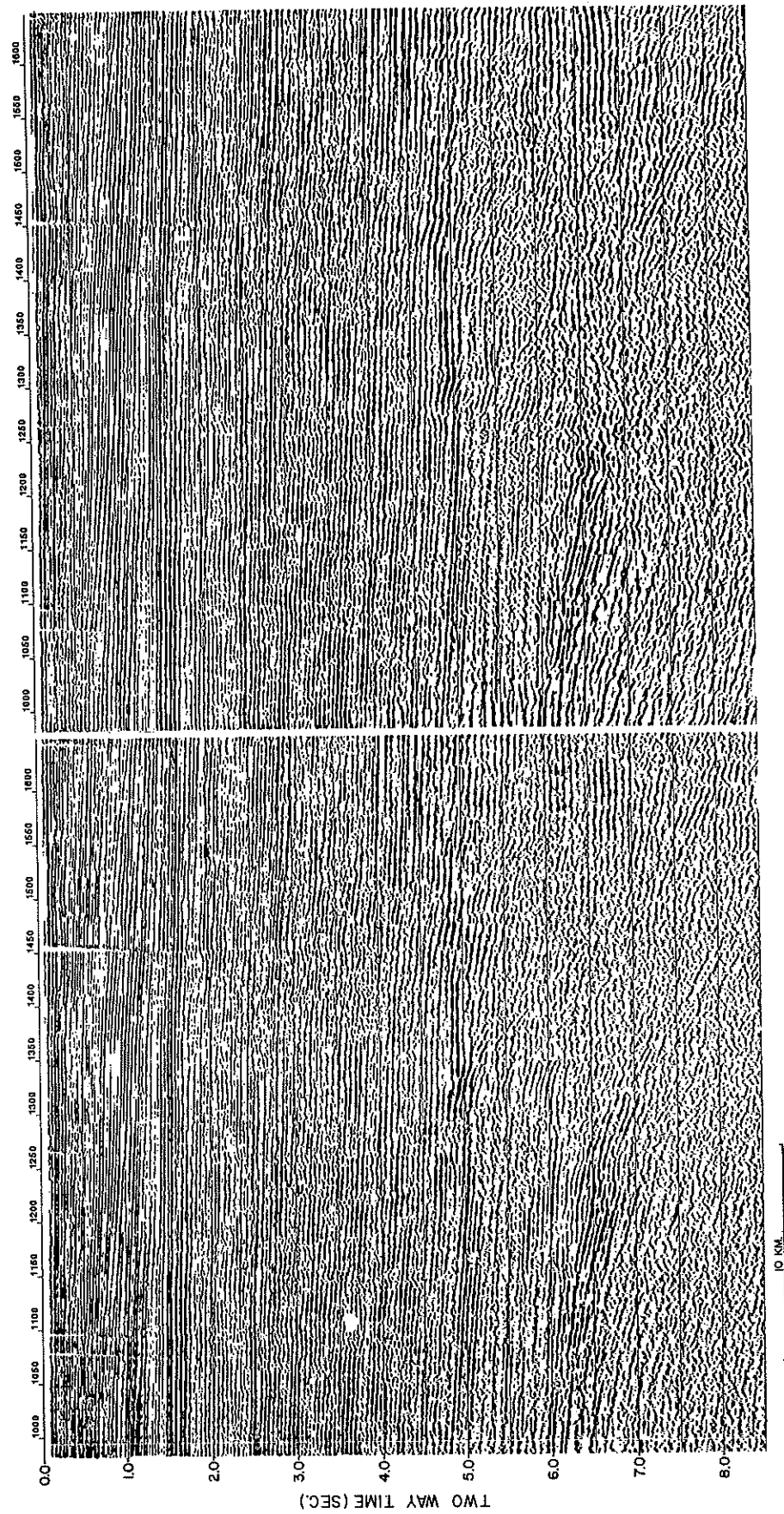


FIGURE 8

Figure 9a LASE Expanding Spread Profile 3A (right) and stacked CDP section (left), where this profile is located at approximately CDP 1620. Although this profile extends to 50 km, we show only the first 20 km.

Figure 9b LASE Expanding Spread Profile 3A, after f-k filtering, designed to eliminate water-borne energy (low phase velocity arrivals). In this record section it is quite clear that the wide angle reflections from 4 to 6.5 seconds can now be followed to the larger offsets. These arrivals' reflection time and offset were digitized and used in T^2-X^2 reflection analysis to derive interval velocities. Of particular interest is the zone between 5 and 6.5 seconds where a velocity of 5.7 km/sec is observed.

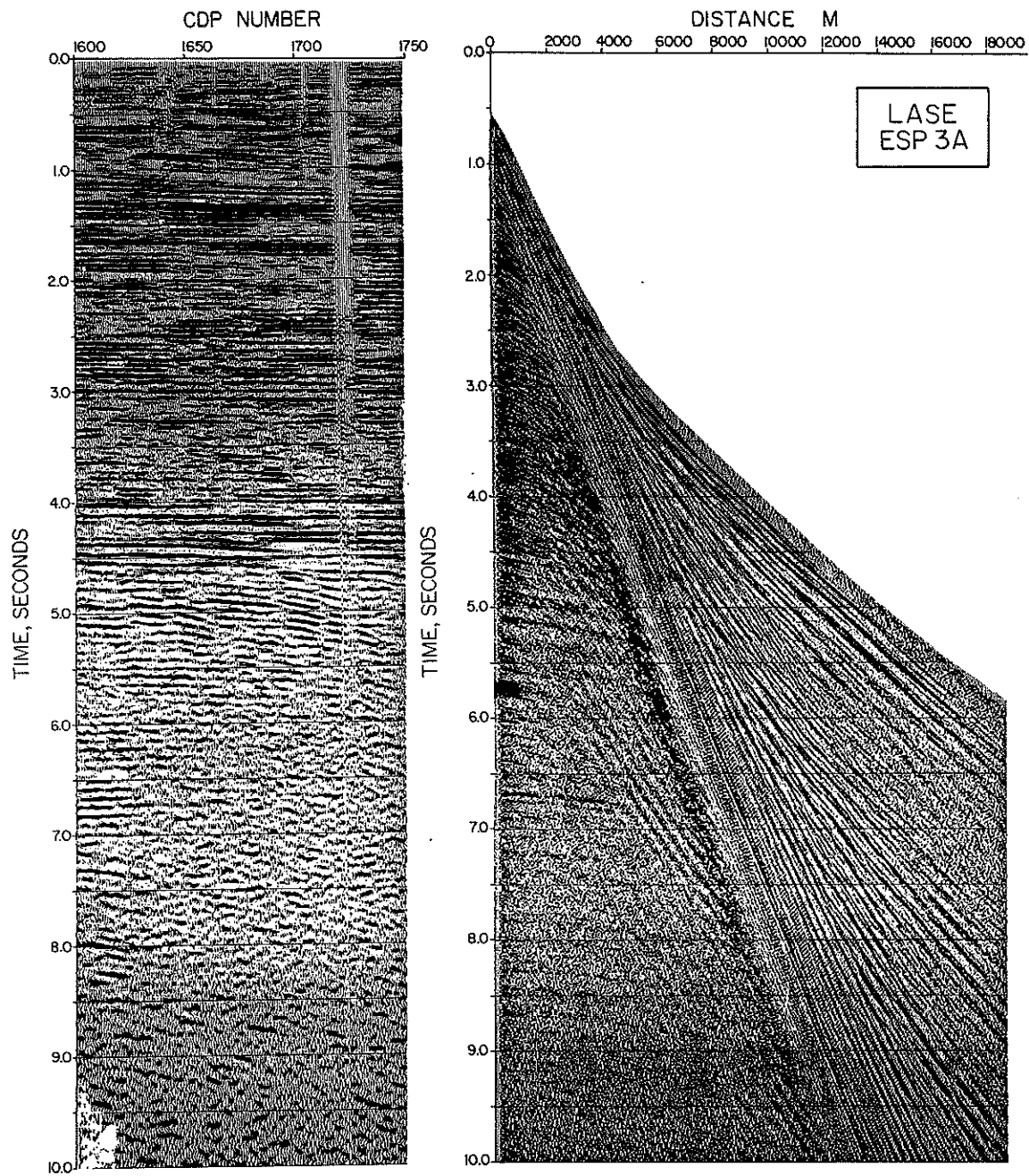


FIGURE 9a

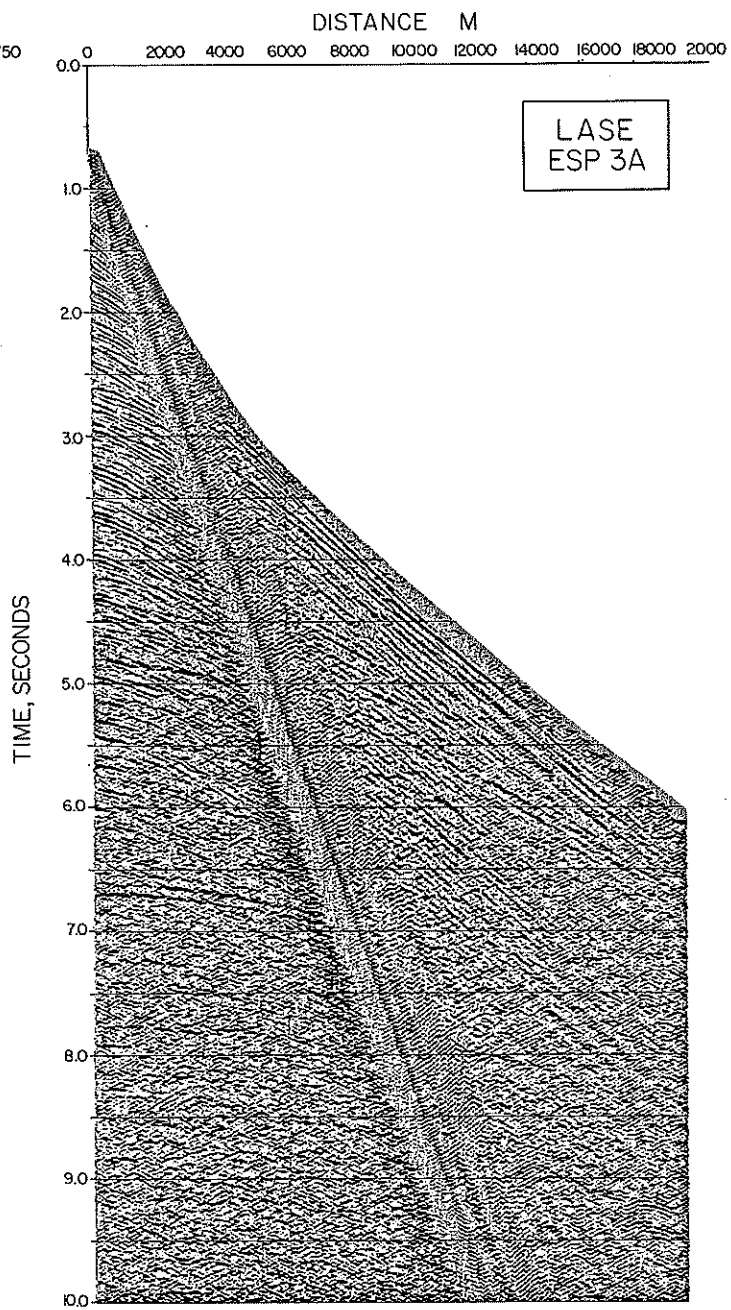
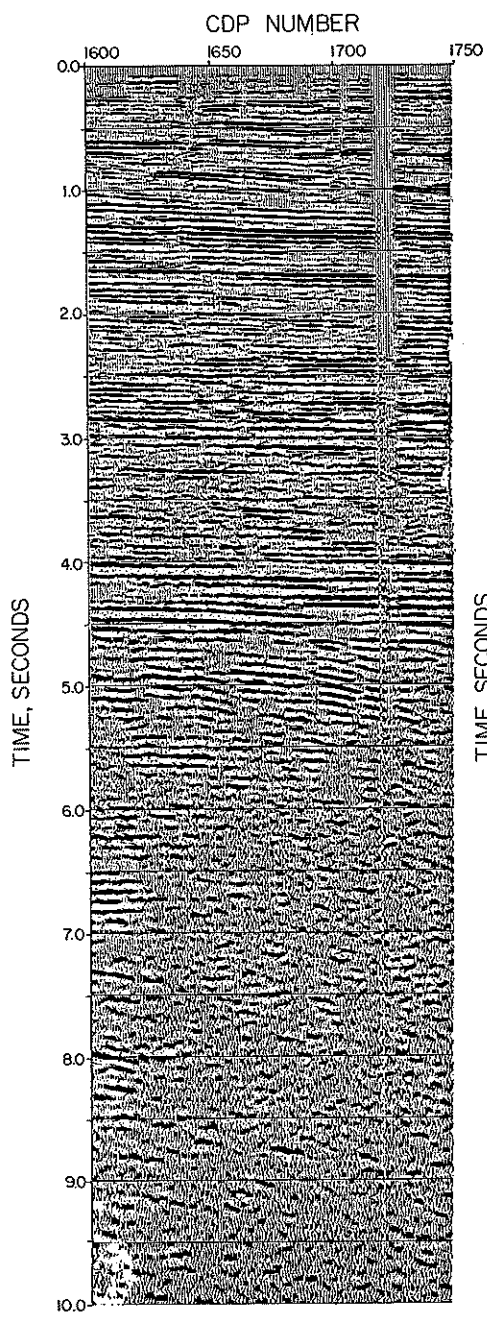


FIGURE 9b

Figure 10

Comparison of the velocity results and methods used in deriving the final solution for ESP 3 and 3A. Interval velocities are shown on the left in terms of traveltime and on the right in terms of depth. The bars on the time section show the limits of the various methods. Since the tau-p method yields the most detail, these results were used for the upper part of the section, after modification to ensure matching of reflections seen in the T-X data. The T^2-X^2 velocities fit quite well, except that they provide no resolution in the shallow part of the section. The closely packed curves reaching down to 2 seconds in time and 3 km in depth are from first arrival analyses from four nearby LASE CDP gathers. (We include these curves here to show how well the results agree.) In the high velocity - low velocity sequence between 4 and 6.5 seconds, the T^2-X^2 results are the "Layercake" model, while the ESP 3 T-X results contain gradients. The principal value of the T^2-X^2 results was in confirming the velocities of the high velocity - low velocity sequence.

LASE ESP 3,3A

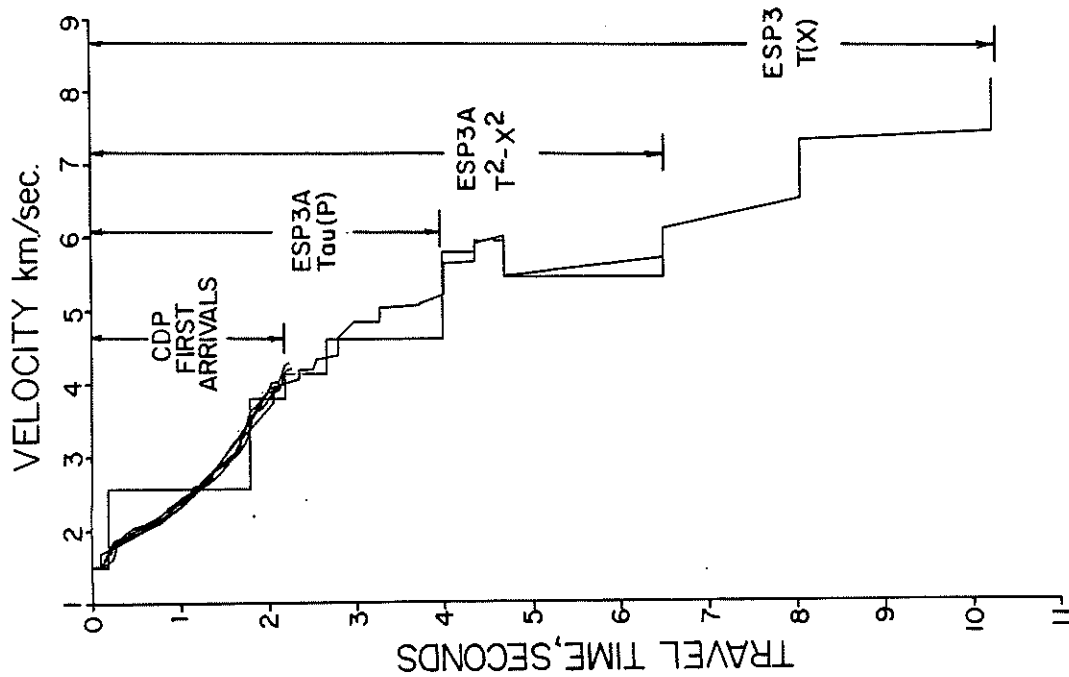
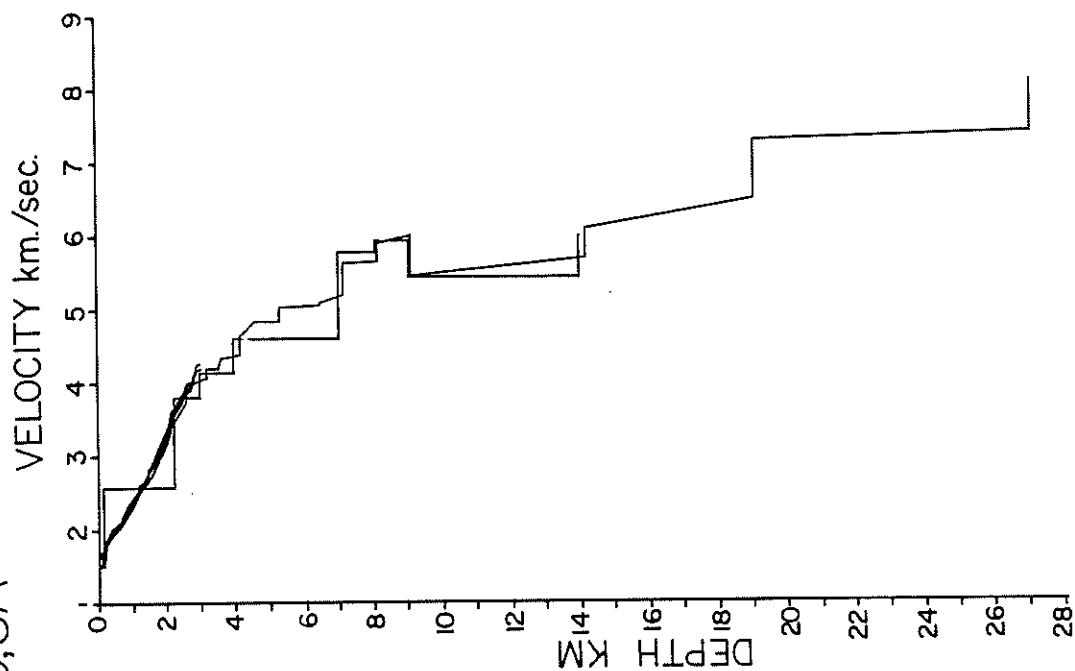


FIGURE 10

Figure 11a LASE airgun Expanding Spread Profile 4A (right) and the CDP stacked record section (left) where this profile is located at approximately CDP number 2320. 50 km of data were recorded, but only the first 20 km are displayed. Strong multiple arrivals, both from the water column and the interval between the seafloor and the top of the carbonate bank are observed and obscure any deep reflection events.

Figure 11b The T-X data of ESP 4A were transformed to the tau-p domain (right) by slant stacking. Picks of critical arrivals on this plot were digitized and inverted to interval velocity by the Tau-Sum method. Velocities for the upper part of the section (0-4 sec) of two-way normal time were thus obtained.

Figure 11c The tau-p data of Figure 12b, corrected to two-way normal time, using the final interval velocity function. The extent to which the reflections follow horizontal trajectories reflects the accuracy of the interval velocity function. The original Tau-Sum velocities were iteratively corrected to produce the result shown here. When velocity gradients are present, the arrivals along the far right edge of the corrected tau-p data cannot be straightened but connect between layers.

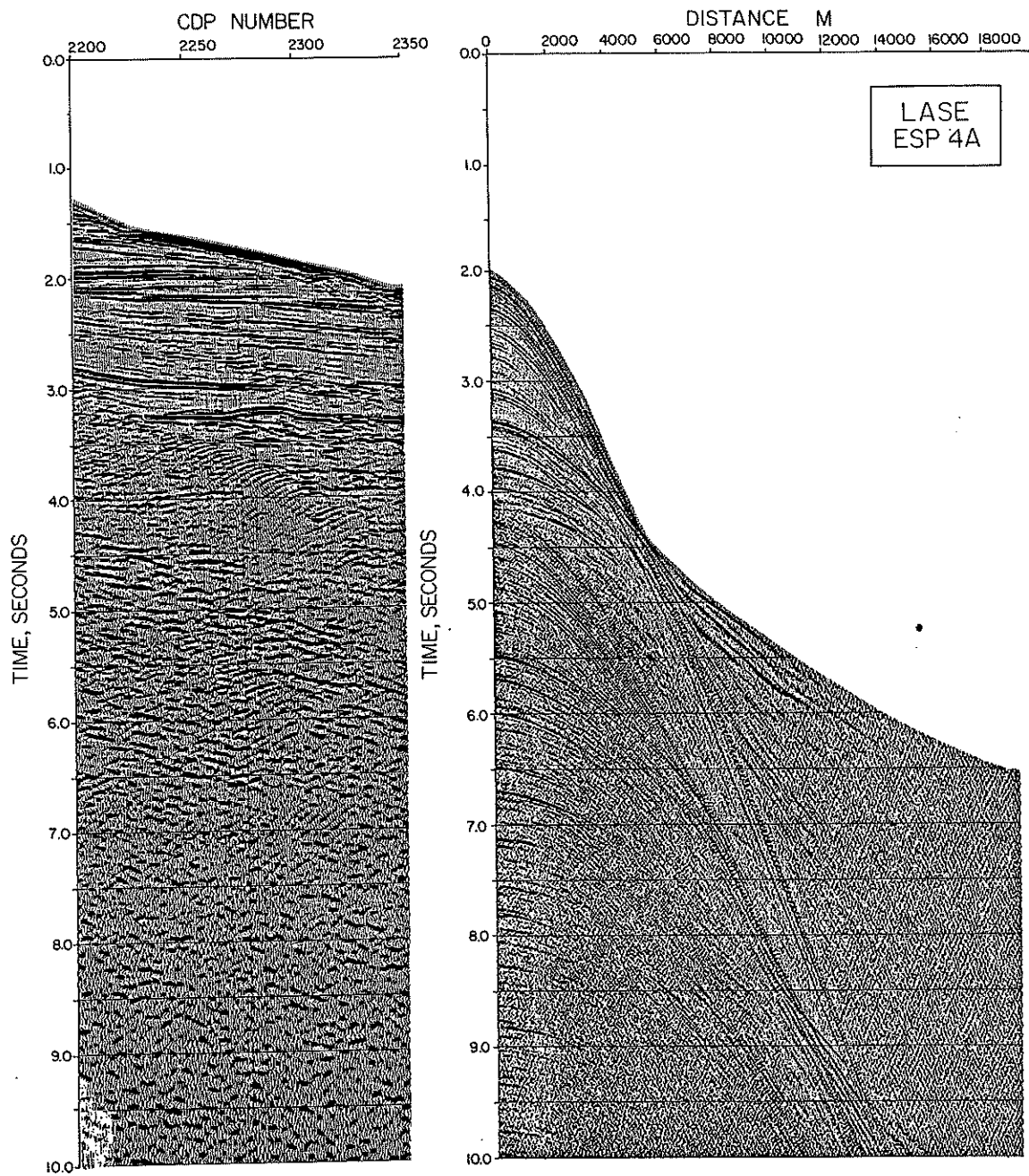


FIGURE 11a

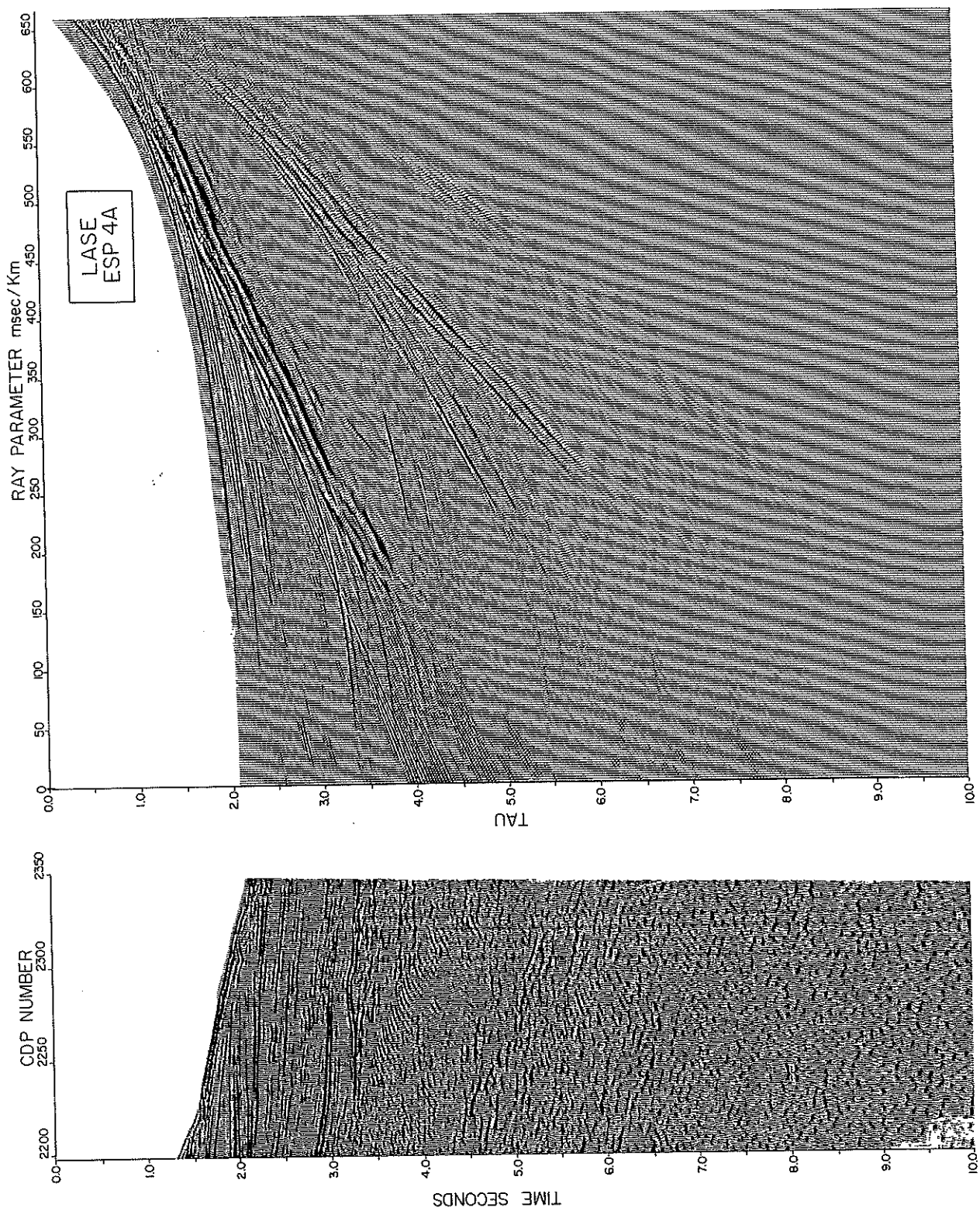


FIGURE 11b

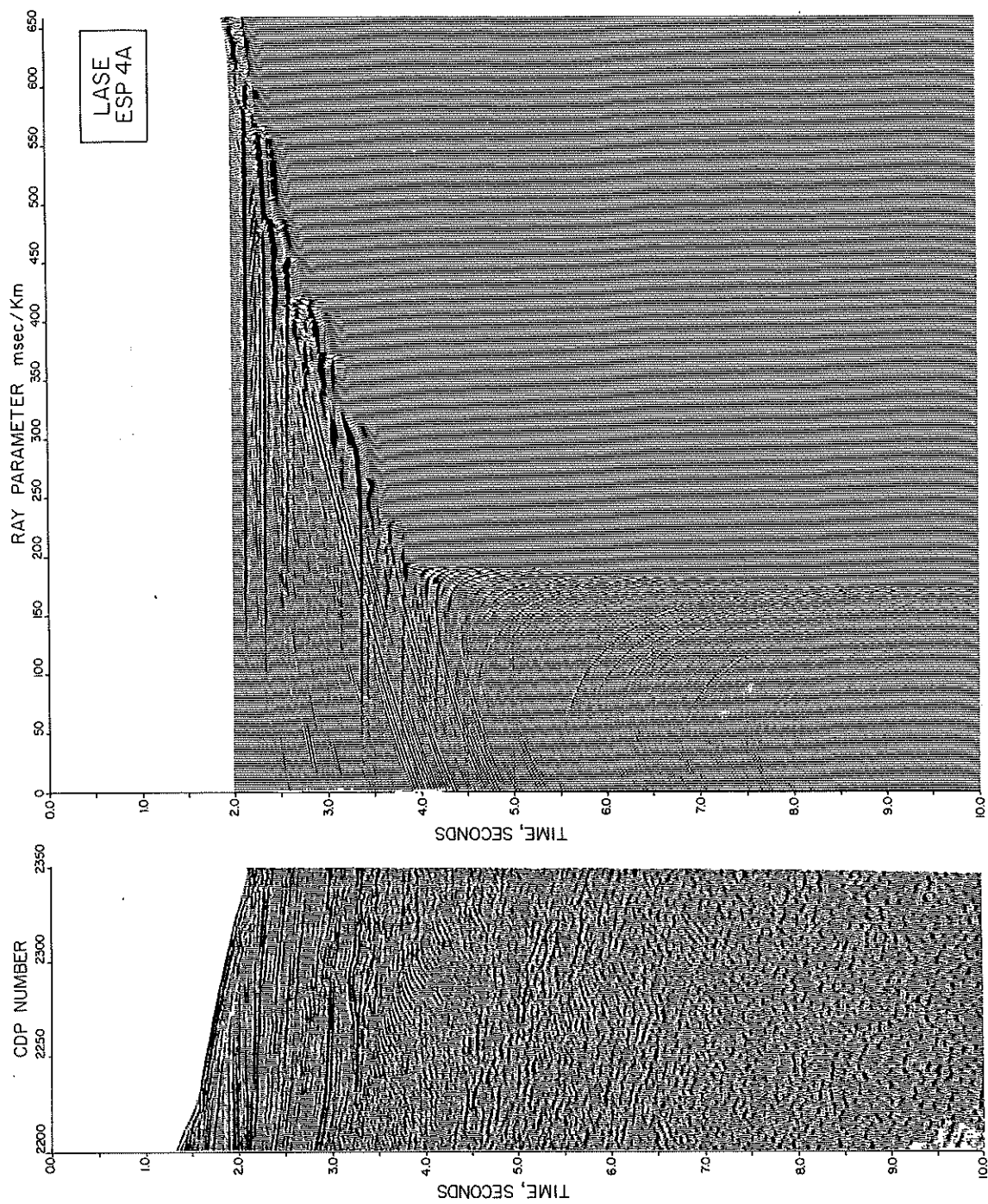


FIGURE 11c

Figure 12 LASE explosive ESP 2 reduced with a velocity of 5.5 km/sec. The traveltimes predicted from the final model are superimposed and the location of the points of critical reflection are marked by arrows.

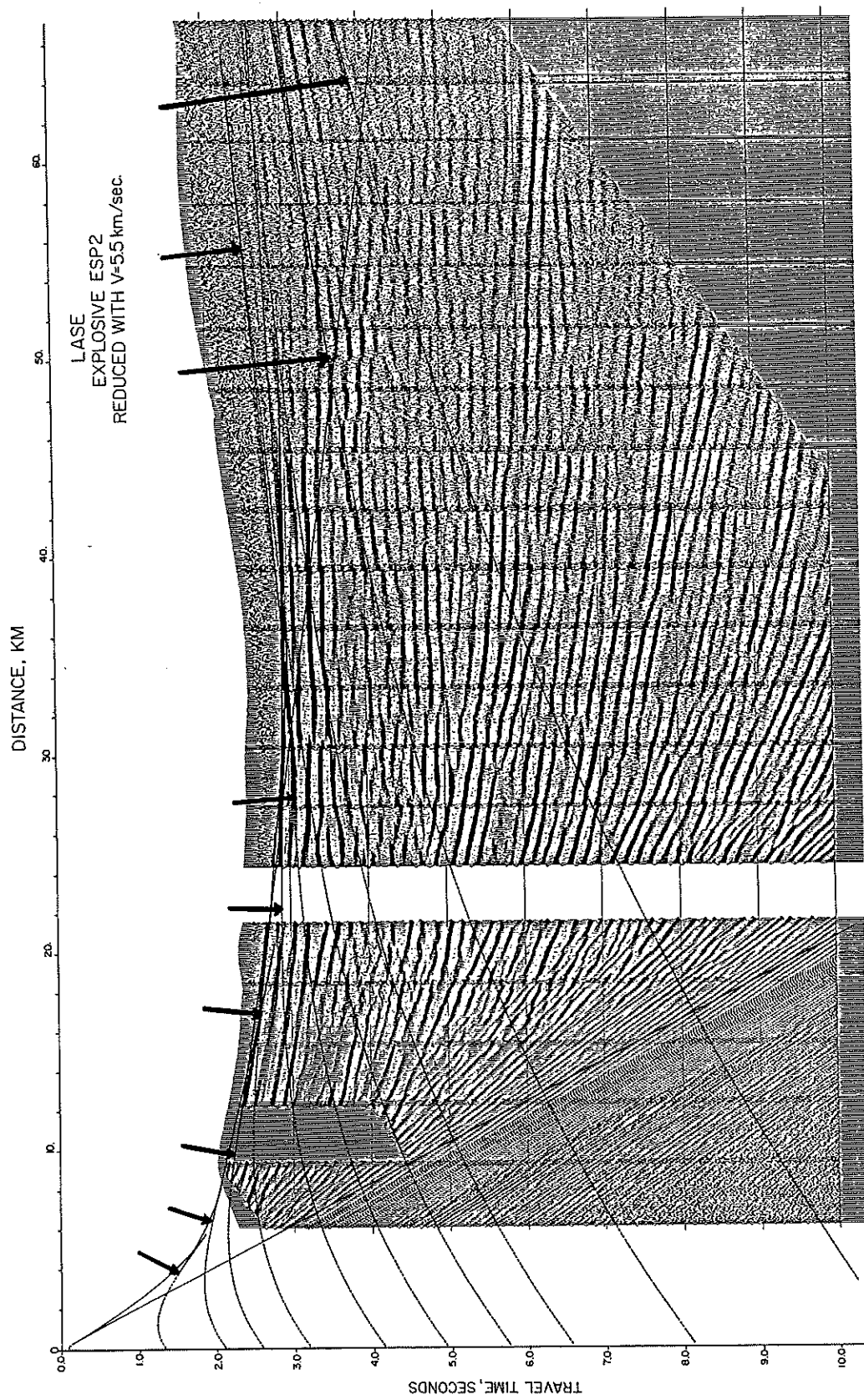


FIGURE 12

Figure 13 Detail of the reflection at 6.5 seconds two-way time at the base of the low velocity zone. On the left the data were corrected for normal moveout with stacking velocities derived from our final velocity function (Figure 10). It is apparent that this deep event, as indicated by the arrows, follows an approximately horizontal trajectory. To test the presence of the low velocity zone, the data were corrected for normal moveout with the same velocity as the layer above. As shown on the right, it is quite clear that this correction is incorrect for the event at 6.5 sec. Since this event is now undercorrected, a lower velocity is required to make the reflection follow a horizontal trajectory. Even on the left, a slightly lower velocity is implied.

LASE ESP 3A NMO

L.V. Zone

OFFSET, km

0

5

10

15

millisec.

6000

6500

7000

millisec.

0

5

10

15

No L.V.Z.

OFFSET, km

0

5

10

15

6000

6500

7000

FIGURE 13